GM-CSF primes cardiac inflammation in a mouse model of Kawasaki disease

Angus T. Stock,[1] Jacinta A. Hansen,[1] Matthew A. Sleeman,[2] Brent S. McKenzie,[3] and Ian P. Wicks[1,4,5]

[1]The Walter and Eliza Hall Institute of Medical Research, Melbourne, Victoria 3052, Australia
[2]Department of Respiratory, Inflammation, and Autoimmunity Research, MedImmune Limited, Cambridge CB21 6GH, England, UK
[3]CSL Limited Research Department, Bio21 Molecular Science and Biotechnology Institute and [4]Department of Medical Biology, University of Melbourne, Melbourne, Victoria 3052, Australia
[5]Rheumatology Unit, The Royal Melbourne Hospital, Parkville, Victoria 3050, Australia

Kawasaki disease (KD) is the leading cause of pediatric heart disease in developed countries. KD patients develop cardiac inflammation, characterized by an early infiltrate of neutrophils and monocytes that precipitates coronary arteritis. Although the early inflammatory processes are linked to cardiac pathology, the factors that regulate cardiac inflammation and immune cell recruitment to the heart remain obscure. In this study, using a mouse model of KD (induced by a cell wall *Candida albicans* water–soluble fraction [CAWS]), we identify an essential role for granulocyte/macrophage colony–stimulating factor (GM-CSF) in orchestrating these events. GM-CSF is rapidly produced by cardiac fibroblasts after CAWS challenge, precipitating cardiac inflammation. Mechanistically, GM-CSF acts upon the local macrophage compartment, driving the expression of inflammatory cytokines and chemokines, whereas therapeutically, GM-CSF blockade markedly reduces cardiac disease. Our findings describe a novel role for GM-CSF as an essential initiating cytokine in cardiac inflammation and implicate GM-CSF as a potential target for therapeutic intervention in KD.

INTRODUCTION

First described in 1967 as an acute febrile syndrome (Kawasaki, 1967), Kawasaki disease (KD) is now recognized as the leading cause of pediatric heart disease in developed countries (Uehara and Belay, 2012; Sundel, 2015). KD causes an acute vasculitis of medium-sized vessels, most commonly involving the coronary arteries. Although the exact pathogenesis of KD remains ill defined, it is believed that an initial inflammatory event causes myocarditis and/or panarteritis, with inflammatory cells infiltrating the heart (Fujiwara et al., 1978; Fujiwara and Hamashima, 1978; Takahashi et al., 2005; Harada et al., 2012). These events disrupt the arterial wall, precipitating the formation of coronary artery aneurysms that appear around 10–14 d after disease onset (Naoe et al., 1991; Takahashi et al., 2011). Disease severity ranges from self-limiting arterial dilatation to giant coronary artery aneurysms. KD is lethal in ∼1% of untreated cases as a result of coronary artery rupture, myocarditis, or myocardial infarction (Fujiwara et al., 1978; Kato et al., 1996; Takahashi et al., 2005; Harada et al., 2012).

Despite extensive research, the etiology of KD remains obscure. A genetic basis is assumed given the increased rate in Asian (∼200/100,000 in Japan) compared with Caucasian (∼20/100,000 in the USA) ethnicity (Holman et al., 2010; Uehara and Belay, 2012). The elevated KD risk is retained in Japanese nationals living abroad, and an increased familial incidence is seen in relatives of KD patients (Sundel, 2015). In keeping with the possibility of genetic susceptibility, genome-wide association study screens have yielded several single nucleotide polymorphisms associated with KD, most notably in immune-related genes. Single nucleotide polymorphisms have been found in *FCGR2a*, *Caspase 3*, *ITPK* (inositol 1,4,5-trisphosphate 3-kinase C), *BLK* (B lymphoid tyrosine kinase), *CD40*, and *HLA* (human leukocyte antigen) *class II* (Onouchi, 2012; Onouchi et al., 2012). However, confirmatory studies substantiating a role for these candidate genes have yet to be performed, and thus, their contribution to KD remains unclear. In addition to a genetic predisposition, KD is thought to require an infectious trigger. KD epidemics have been documented (1979, 1982, and 1986), and seasonal variations are also observed (peaking in winter/autumn), consistent with an infectious agent (Kawasaki, 2006; Principi et al., 2013). However, although preceding bacterial, fungal, or viral infections have been reported in KD patients (Principi et al., 2013), no common microbial pathogen has emerged. Thus, the prevailing hypothesis is that KD results from an infection (with numerous possible microbial culprits) eliciting an exaggerated inflammatory response in genetically predisposed children

that, for unknown reasons, manifests as vasculitis, peculiarly localized to the heart.

The immune system is thought to be the primary mediator of the pathogenesis of KD. CD8^{+} T cells and B cells have been reported in varying degrees in the coronary artery lesions of KD patients (Brown et al., 2001; Takahashi et al., 2005; Harada et al., 2012). However, it is noteworthy that KD is nonrecurring and, hence, unlikely to involve persistent autoreactive T or B cell responses against self-antigens. Instead, the innate arm of the immune system is believed to be the major mediator of heart disease. Histological analyses of autopsied KD patients reveal that monocytes/macrophages and neutrophils are the major immune cell populations within coronary arterial lesions (Fujiwara et al., 1978; Takahashi et al., 2005; Harada et al., 2012). The appearance of neutrophils and monocytes in the heart precedes coronary arteritis, suggesting direct involvement in the initiation of cardiac pathology (Takahashi et al., 2005). In line with a pathogenic role, neutrophils and monocytes increase in number and function during the acute phase of KD, expressing high levels of effector molecules such as nitric oxide, reactive oxygen species, neutrophil elastase, vascular endothelial growth factors, and matrix metalloproteinases (MMPs; Niwa and Sohmiya, 1984; Hamamichi et al., 2001; Biezeveld et al., 2005; Senzaki, 2006; Yoshimura et al., 2009; Korematsu et al., 2012). It has been argued that invading neutrophils and monocytes drive intimal cell proliferation and the destruction of the elastic lamina via the release of such factors, resulting in disruption of the arterial wall and formation of coronary aneurysms.

It is clearly critical to understand how the migration of neutrophils and monocytes into the heart is regulated during KD. However, although several cytokines and immune mediators (such as TNF, granulocyte CSF [G-CSF], vascular endothelial growth factors, and MMPs) are elevated in the peripheral blood during acute KD (Matsubara et al., 1990; Hamamichi et al., 2001; Suzuki et al., 2001; Biezeveld et al., 2005), which factors regulate local tissue inflammation within the heart remains poorly described. As such, a comprehensive assessment of the factors that activate cardiac inflammation during KD is required. To this end, we have used the *Candida albicans* water-soluble fraction (CAWS) experimental mouse model of KD. This model originated from findings that *C. albicans* isolated from KD patients could induce coronary arteritis in mice (Murata and Naoe, 1987), an activity that was enriched in the water-soluble fraction of *Candida* yeast (Nagi-Miura et al., 2006). Using this model, we discovered a surprising role for GM-CSF as the primary activating cytokine of cardiac vasculitis during KD. GM-CSF was expressed locally within the heart during the initial phase of disease, triggering cardiac inflammation via the activation of resident myeloid cells. Our findings describe a novel role for this pathway in cardiac inflammation and implicate GM-CSF as a potential target for therapeutic intervention in KD and related vasculitides.

RESULTS

CAWs induces a biphasic, cardiac–specific inflammation in mice

We investigated the CAWS model of KD. The CAWS complex is a carbohydrate-rich, water-soluble fraction of *C. albicans*, comprised mainly of cell wall–derived α-mannans and β-glucans (Saijo et al., 2010). CAWS is recognized by the C-type lectin receptor Dectin-2 and signals via an Fcγ–Syk–CARD9 pathway (Saijo et al., 2010; Kerscher et al., 2013). We initially characterized the CAWS model of KD in C57BL/6 (B6) mice. In line with earlier studies (Murata and Naoe, 1987; Nagi-Miura et al., 2006), the i.p. injection of CAWS elicited cardiac vasculitis, characterized by a cellular infiltrate that localizes to the aortic root and coronary arteries of the heart by 1 mo after injection (Fig. 1, a and b). We next used flow cytometry to more precisely enumerate and characterize the cardiac infiltrate. To restrict analysis to cells that had entered the heart, we used an in vivo labeling technique, injecting a fluorochrome-conjugated anti–GR-1 antibody i.v. just before sacrifice. Using this approach, monocytes and neutrophils in the circulation and vasculature are exposed to and labeled by the anti–Gr-1 antibody, whereas cells within the tissue are not, allowing discrimination between circulating (in vivo Gr-1^{+}) and tissue-resident (in vivo Gr-1^{−}) cells (Ng et al., 2011; Stock et al., 2014). We found that in the steady state, the heart is largely devoid of neutrophil and monocytes, but there is a major myeloid population of CD11b^{+}Ly6C^{−}Ly6G^{−} cardiac macrophages that express CD64 and variable levels of MHC class II (Fig. 1 c). After CAWS challenge, large populations of CD11b^{+}Ly6C^{+}Ly6G^{+} neutrophils and CD11b^{+}Ly6C^{hi}Ly6G^{−} monocytes traffic into the heart. Phenotypic analysis showed that Ly6C^{hi} monocytes express CD64^{+} but little MHC class II, whereas Ly6G^{+} neutrophils express neither. A kinetic analysis of neutrophil and monocyte infiltration revealed a biphasic pattern of cardiac inflammation after CAWS challenge. Specifically, there was an early, short-lived influx of neutrophils and monocytes into the heart 1 d after CAWS challenge, followed by a second neutrophil–rich infiltrate, emerging ∼28 d later, which persisted for several weeks (Fig. 1 d). Comparing the location of neutrophils in the heart by immunohistochemistry (IHC) during the initial (day 1) and second wave (day 28) of disease revealed that neutrophils were distributed evenly throughout the heart 1 d after CAWS challenge but had localized to the aortic root and coronary arteries by day 28 (Fig. 1 e). In line with this finding, FACS analysis of dissected heart quadrants showed that neutrophils localized with equivalent frequency in all quadrants at day 1 after CAWS but were highly enriched in the upper quadrants of the heart (i.e., in the region of the aortic root and coronary arteries) at day 28 (Fig. 1 f). Thus, in keeping with human KD, where an initial, diffuse myocarditis precedes coronary arteritis (Fujiwara and Hamashima, 1978; Dahdah, 2010; Harada et al., 2012), CAWS challenge elicits a rapid invasion of neutrophils and monocytes throughout the myocardium that is followed by a
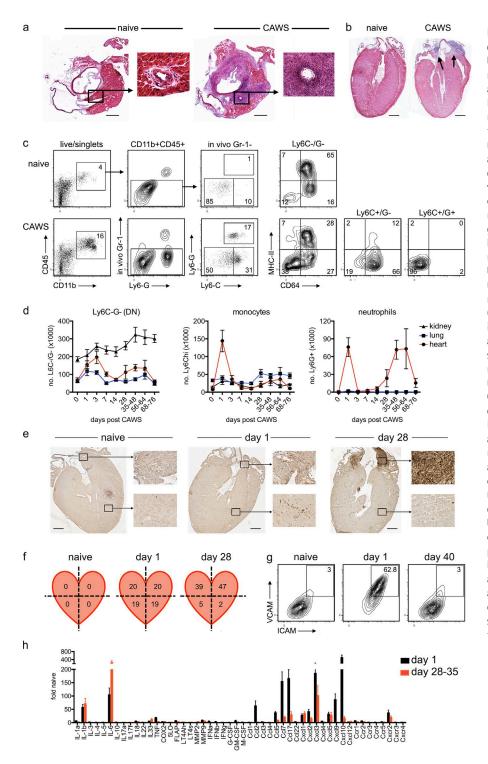
Figure 1. **CAWS induces a biphasic, cardiac-specific inflammation in mice.** (a and b) C57BL/6 (B6) mice were injected i.p. with 4 mg CAWS. 28 d later, mice were euthanized, and the hearts were excised for HE staining. Representative image (of hearts from 7 to 88 mice over at least four experiments) cut on a transverse (a) or coronal (b) plane are shown (cropped images show coronary arteries, and arrows indicate infiltrate). Bars, 1 mm. (c and d) B6 mice were injected with CAWS, and at various times, hearts were analyzed by flow cytometry (mice received anti–Gr-1 PE i.v. 10 min before sacrifice to prelabel circulating granulocytes). (c) Representative FACs plots of hearts from naive and day 1 CAWS-challenged mice are shown. (d) A time course for the number of Ly6C$^-$/G$^-$ (double negative [DN]) myeloid (CD45.2$^+$/CD11b$^+$/in vivo GR-1$^-$/Ly6C$^-$/Ly6G$^-$), monocytes (CD45.2$^+$/CD11b$^+$/in vivo Gr-1$^-$/Ly-6C^{hi}/Ly6G$^-$), and neutrophils (CD45.2$^+$/CD11b$^+$/in vivo Gr-1$^-$/Ly6C$^+$/Ly6G$^+$) in the heart, lung, and kidney of B6 mice after CAWS challenge is shown (data depict the mean ± SEM of 5–17 mice pooled from at least two experiments). (e and f) Hearts were isolated from naive or CAWS-challenged B6 mice (injected 1 or 28 d earlier) and either stained with anti-Ly6G for IHC (bars, 1 mm; e) or dissected into quadrants, and the frequency of neutrophils in each quadrant were analyzed by flow cytometry (values are mean percent Ly6G$^+$ of CD11b$^+$/CD45.2$^+$ of five to six mice from two experiments; f). (g) The expression of ICAM and VCAM on cardiac endothelium (CD45$^-$CD31$^+$) was analyzed by flow cytometry (inset values show the mean of 9–12 mice pooled from at least three experiments). (h) Hearts from B6 mice were harvested 1 or 28–35 d after CAWS challenge and assessed by qPCR (gene expression is relative to naive controls and the mean ± SEM of five mice from two to three experiments is shown). FLAP, 5-lipoxygenase activating protein; M-CSF, macrophage CSF.

second, delayed inflammatory infiltrate that targets the aortic root and coronary arteries.

We next evaluated cardiac vasculitis in more detail. CAWS challenge induced rapid activation of cardiac endothelium, as seen by the up-regulation of intercellular adhesion molecule (ICAM) and vascular cell adhesion molecule (VCAM; Fig. 1 g). Furthermore, transcriptional analysis of hearts removed on day 1 or 28 revealed that several inflammatory cytokines (*IL-1β* and *IL-6*) and chemokines (*Ccl2/7/17*, *Cxcl1-3*, and *Cxcl9/10*) were strongly up-regulated during one or both phases of disease (Fig. 1 h), consistent with the development of local cardiac inflammation. Critically, although we consistently found cardiac inflammation after CAWS injection, these events were restricted to the heart.

Specifically, at no point did neutrophils enter the lung or kidney after CAWS (Fig. 1 d), and we did not see marked endothelial activation in these tissues (not depicted). In summary, we find that CAWs induces a biphasic, cardiac-specific vasculitis, characterized by neutrophil and monocyte infiltrate, endothelial activation, and local inflammatory cytokine/chemokine expression. These features are in keeping with what is described for human disease, arguing that this is an informative model for KD.

GM–CSF deficiency protects against the development of cardiac disease in the CAWS model of KD

We next examined which cytokines and cell types drive cardiac inflammation after CAWS challenge. To this end, we challenged a panel of cytokine and receptor KO mice with CAWS, and 1 d later, we measured neutrophil and monocyte infiltrate into the heart, together with ICAM/VCAM expression on cardiac endothelium. As seen in Fig. 2, mice deficient in IL-1, IL-17A, or G-CSF signaling developed robust cardiac inflammation after CAWS challenge with neutrophil and monocyte infiltrate, plus endothelial activation, that was equivalent to control animals. IL-6–deficient mice had a mild (albeit significant) reduction in neutrophil and monocyte infiltrate and, paradoxically, elevated levels of ICAM/VCAM expression on cardiac endothelium. At face value, these findings argue that IL-1, IL-6, IL-17, and G-CSF signaling are not essential for the development of cardiac vasculitis. Rag-γc$^{-/-}$ mice also developed typical cardiac inflammation, indicating that lymphoid cells are not required for the initial cardiac vasculitis. In contrast, mice deficient in GM-CSF did not develop any signs of cardiac inflammation. GM-CSF$^{-/-}$ mice had no neutrophil and minimal monocytic infiltrate into the heart and significantly reduced endothelial activation after CAWS challenge (Fig. 2, a–e). Furthermore, GM-CSF$^{-/-}$ mice showed minimal expression of the inflammatory genes that emerge in cardiac tissue of WT mice after CAWS challenge (Fig. 2 f), indicating virtually complete absence of inflammation in the heart. Given that CAWS induces a biphasic pattern of cardiac inflammation (Fig. 1 d), we next examined whether GM-CSF$^{-/-}$ mice were also protected from the second wave of disease. In keeping with protection from the initial wave of cardiac inflammation, GM-CSF mice did not develop a secondary neutrophil infiltrate at 28–40 d after challenge, as assessed by hematoxylin and eosin (HE) staining and flow cytometry (Fig. 2, g–i). Overall, these findings identify an essential role for GM-CSF in the development of inflammatory cardiac disease in the CAWS model of KD.

Local GM–CSF expression activates cardiac inflammation in the CAWS model of KD

We next investigated where and when GM-CSF operates to drive cardiac vasculitis in KD. Neutralizing GM-CSF (with anti–GM-CSF antibodies) at the time of CAWS challenge in WT mice blocked the development of cardiac vasculitis, potently reducing neutrophil and monocyte migration into the

heart and attenuating endothelial activation (Fig. 3, a and b). This finding indicates that the induction of GM-CSF expression after CAWS challenge is essential for the development of cardiac disease, and hence, it operates as an effector cytokine in the context of this disease. Critically, sustained GM-CSF blockade also protected mice against the development of CAWS-induced vasculitis at day 28 (Fig. 3, c and d), highlighting the therapeutic potential of GM-CSF antagonists in KD.

We next asked whether GM-CSF was involved in the systemic response to CAWS challenge or operated selectively in the heart. The i.p. injection of CAWS elicits an initial peritoneal response, as seen by the rapid arrival of neutrophils into the peritoneum (Fig. 3 e). The cardiac response lags behind CAWS-induced peritonitis, with neutrophils entering the heart between 6 and 24 h after challenge. Comparing the peritoneal and cardiac response in WT and GM-CSF$^{-/-}$ mice, we found that although GM-CSF deficiency completely abrogated neutrophil recruitment into the heart, the peritoneal response to CAWS challenge was intact (Fig. 3 f). This finding demonstrates that GM-CSF$^{-/-}$ mice do respond to the CAWS challenge but are unable to recruit neutrophils into the heart, suggesting that GM-CSF acts locally to initiate cardiac inflammation. In line with this finding, *GM-CSF* was rapidly expressed in the heart after CAWS challenge, peaking at ∼6 h after challenge (Fig. 3 g). Notably, GM-CSF expression precedes the arrival of neutrophils into the heart, consistent with an initiating role. Furthermore, examination of a range of tissues showed that *GM-CSF* up-regulation occurs in the heart but not elsewhere in the body (BM, LN, spleen, or lung) after CAWS challenge (Fig. 3 h), arguing that GM-CSF acts selectively within the heart. Collectively, these findings demonstrate that (a) GM-CSF is an essential inflammatory cytokine in the development of inflammatory cardiac disease in the CAWS model of KD, and (b) GM-CSF is expressed and acts locally in the heart to drive cardiac inflammation.

Cardiac fibroblasts (CFs) are the major source of GM–CSF within the heart

The data shown in Fig. 3 indicate that locally produced GM-CSF selectively activates cardiac inflammation upon CAWS challenge. We therefore examined the source of GM-CSF in the heart, generating reciprocal GM-CSF KO BM chimeras to determine whether GM-CSF was produced by the BM and/or the parenchymal compartment. WT recipients of either WT or GM-CSF$^{-/-}$ BM developed cardiac vasculitis after CAWS challenge, as assessed by neutrophil/monocyte infiltrate and endothelial activation, whereas GM-CSF$^{-/-}$ recipients of either WT or GM-CSF$^{-/-}$ BM were protected (Fig. 4, a and b). These results show that GM-CSF is produced by a radio-resistant source during disease initiation. To more precisely identify the cellular source, we measured GM-CSF expression in purified leukocytes, endothelial cells, fibroblasts, and CD31$^-$gp38$^-$ stromal cells sorted from the hearts of naive and CAWS-challenged mice (Fig. 4 c). Consistent with production by a radio-resistant, non–BM-derived
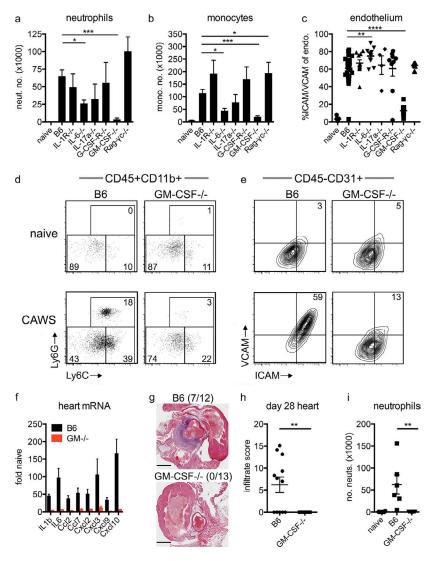
Figure 2. **GM-CSF is essential for the development of cardiac disease in the CAWS model of KD.** (a–e) B6 and KO mice were injected with CAWS, and 1 d later, the hearts were analyzed for neutrophil (neut.; a) and monocyte (mono.; b) infiltrate and ICAM/VCAM expression on endothelium (endo.; c) by flow cytometry. FACs plots show Ly6C and Ly6G are gated on heart-resident (in vivo Gr-1$^-$) myeloid cells (CD11b$^+$/CD45.2$^+$; d) and ICAM/VCAM expression on endothelium (CD45.2$^-$CD31$^+$; e). Data depict the mean ± SEM from 4 to 30 mice pooled from at least two experiments. (f) Inflammatory gene expression from the hearts of B6 and GM-CSF$^{-/-}$ mice was assessed by qPCR 1 d after CAWS challenge (values are relative to naive B6 hearts and show the mean ± SEM of six mice from two experiments). (g and h) B6 and GM-CSF$^{-/-}$ mice were challenged with CAWS, and 28–40 d later, the hearts were analyzed for infiltrate by HE staining and flow cytometry. Representative HE images with inflammatory infiltrate incidence (in parentheses; g) and infiltrate score (h) are shown (pooled from two experiments). Bars, 1 mm. (i) Cardiac neutrophil infiltrate enumerated by flow cytometry (individual mice are shown pooled from two experiments). Statistical analysis was performed with unpaired, two-tailed Student's t tests. *, P < 0.05; **, P < 0.01; ***, P < 0.001; ****, P < 0.0001.

source, CD45$^-$CD31$^-$gp38$^+$ CFs were the only population to up-regulate GM-CSF in response to CAWS challenge (Fig. 4 d). Intriguingly, CFs also expressed high levels of Ccr2 chemokine ligands *Ccl2* and *Ccl7* compared with other cardiac cells but had comparable or lower expression of other cytokines such as *IL-1β*, *IL-6*, and *TNF*. Importantly, the up-regulation of *GM-CSF* was restricted to fibroblasts of the heart, as fibroblasts sorted from the lung or LNs of CAWS-challenged mice did not show increased *GM-CSF* expression (Fig. 4 e). Furthermore, CFs expressed *GM-CSF* at day 1 after CAWS (Fig. 4 f) but not at day 28 (i.e., the second phase of disease), suggesting GM-CSF is not expressed throughout the second phase of disease. The data shown in Fig. 4 indicate that GM-CSF is rapidly expressed by fibroblasts of the heart but not other organs, driving the initial phase of cardiac inflammation in CAWS-induced KD. In line with rapid cytokine production, CFs exhibited early phenotypic features of activation, up-regulating ICAM and VCAM within 6 h of CAWS challenge (Fig. 4 g). Collectively, these

findings suggest that radio-resistant CFs are rapidly activated upon CAWS challenge and respond by producing GM-CSF that triggers cardiac inflammation.

Activating stimuli and location of CFs

Our results suggest CF-derived GM-CSF triggers cardiac inflammation. We therefore examined how CFs are activated and the location of these cells within the heart. To identify potential stimuli that drive GM-CSF production, we used primary human CF lines. CFs derived from two separate donors up-regulated *GM-CSF* in response to LPS, TNF, and, to varying degrees, CAWS stimulation (Fig. 5 a). Similar results were obtained with mouse CFs (Fig. 5 c), confirming that CFs across species produce GM-CSF and in response to a range of stimuli including TLR ligands, cytokines, and potentially CAWS directly. We next determined the location of CFs within the heart, examining their position in the upper and lower ventricles of naive and CAWS-challenged mice. Sections of the heart were stained with anti-gp38 (or isotype
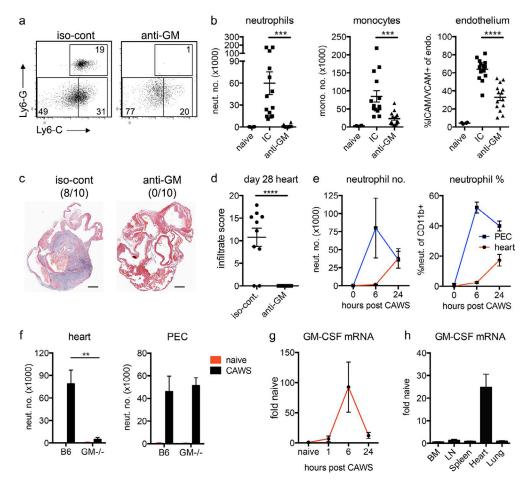
Figure 3. Locally expressed GM–CSF induces cardiac inflammation after CAWS challenge. (a and b) B6 mice were challenged with CAWS and immediately injected with anti–GM-CSF (anti-GM) or isotype control (iso-cont or IC) antibodies. 1 d later, hearts were harvested and analyzed by flow cytometry. Dot plots are gated on heart-resident (in vivo Gr-1⁻) myeloid cells (CD11b⁺/CD45.2⁺; a), and graphs depict neutrophil (neut.) and monocyte (mono.) infiltrate and ICAM/VCAM expression on endothelium (endo.; data points depict individual mice pooled from four experiments; b). (c and d) CAWS-challenged B6 mice were injected with anti–GM-CSF or isotype control antibodies at the time of challenge and then three times weekly. 28 d later, hearts were analyzed by HE staining. A representative section with infiltrate incidence (in parentheses; c) and infiltrate score (d) is shown ($n = 10$ mice pooled from two experiments). Bars, 1 mm. (e) B6 mice were challenged with CAWS, and 6 or 24 h later, neutrophils were enumerated in the heart and peritoneal cavity (PEC) by flow cytometry (data represent four to six mice from two experiments). (f) B6 or GM-CSF⁻/⁻ mice were challenged with CAWS, and 1 d later, neutrophils were enumerated in the heart and peritoneal cavity by flow cytometry (data represent three to nine mice from three experiments). (g) B6 mice were challenged with CAWS, and GM-CSF mRNA were measured in the heart at various times by qPCR (data represent five to six mice pooled from two experiments). (h) B6 mice were challenged with CAWS, and 7–8 h later, various organs were isolated from naive and CAWS-injected mice and assessed for GM-CSF expression by qPCR (data represent five mice pooled from three experiments). GM-CSF mRNA expression levels are shown relative to naive B6 tissue controls. (e–h) Data depict the mean ± SEM. Statistical analysis was performed with unpaired, two-tailed Student's t tests. **, $P < 0.01$; ***, $P < 0.001$; ****, $P < 0.0001$.

control), MHC II, and CD31 antibodies to identify CFs, macrophages, and endothelial cells, respectively. Experiments were performed with RAG-1⁻/⁻ mice to exclude the presence of MHC II⁺ B cells. As seen in Fig. 5 (d–g), gp38⁺ fibroblasts were present in the hearts of naive and CAWS-challenged mice and in both upper and lower regions of the ventricles, although they were more abundant in the former. In regards to distribution within the myocardium, gp38⁺ fibroblasts appeared to cluster in perivascular areas around medium- and small-sized vessels. Furthermore, fibroblasts were found near or adjacent to cardiac macrophages, arguing for potential

local interactions. Collectively, these findings confirm that human and mouse CFs produce GM-CSF in response to a range of stimuli and show that CFs reside in proximity to the vasculature, a location that may explain the ability to induce cardiac vasculitis.

GM-CSF acts on the hematopoietic compartment to drive downstream neutrophil and monocyte recruitment

We next investigated the mechanism by which GM-CSF drives cardiac inflammation. Considering the proximity of GM-CSF–producing CFs to both macrophages and the en-
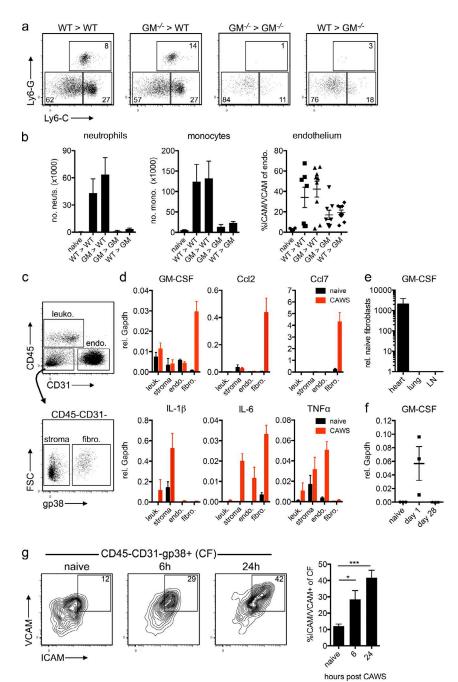
Figure 4. **Radio-resistant CFs produce GM-CSF after CAWS challenge.** (a and b) Reciprocal B6.Ly5.1 (WT) and GM-CSF$^{-/-}$ (GM$^{-/-}$) BM chimeras were challenged with CAWS, and 1 d later, the hearts were analyzed for cardiac vasculitis. (a) Dot plots are gated on heart-resident (in vivo Gr-1$^-$) myeloid cells (CD11b$^+$). (b) Graphs depict the mean ± SEM number of neutrophils (neuts.) and monocytes (mono.) and ICAM/VCAM expression on cardiac endothelium (endo.; data are pooled from four to nine mice from four experiments). (c and d) Hearts from naive or CAWS-challenged mice (6 h after injection) were sorted into CD45$^+$ leukocytes (leuko.), CD45$^-$CD31$^+$ endothelial cells, CD45$^-$gp38$^+$ CFs, and CD45$^-$CD31$^-$gp38$^-$ stromal cells (stroma), and the expression of cytokines and chemokines was analyzed by qPCR. (d) Bar graphs show mean ± SEM gene expression relative (rel.) to Gapdh pooled from three experiments. fibro., fibroblasts; FSC, forward side scatter. (e) Fibroblasts (CD45$^-$CD31$^-$gp38$^+$) were sorted from the heart, lung, and LN of naive and CAWS (∼10 h after challenge) mice, and GM-CSF expression was measured by qPCR. Expression is normalized to naive tissue fibroblasts and shows the mean ± SEM from two experiments (n = 5–6 mice). (f) The expression of GM-CSF by CFs sorted from naive, day 1, or day 28 CAWS-challenged mice was measured by qPCR. Data points show individual experiments (n = 2–3 mice per experiment), with the mean ± SEM indicated. (g) The expression of ICAM and VCAM on CFs was analyzed at various stages after CAWS challenge. FACS plots are gated on CFs (CD45$^-$CD31$^-$gp38$^+$), and graphs depict the mean ± SEM of four to six mice pooled from two experiments. Statistical analysis was performed with unpaired, two-tailed Student's t tests. *, P < 0.05; ***, P < 0.001.

dothelium, we first determined the target of GM-CSF in the CAWS model of KD. Here, we used βc$^{-/-}$ mice that lack the high-affinity common β-chain (CD131) of the GM-CSF, IL-3, and IL-5 receptors. We generated reciprocal BM chimeras to restrict GM-CSF signaling to either BM or parenchymal compartments. After CAWS challenge, we found that both WT and βc$^{-/-}$ hosts receiving WT BM had pronounced cardiac neutrophil and monocyte infiltrate and endothelial activation, whereas WT and βc$^{-/-}$ hosts receiving βc$^{-/-}$ BM were protected (Fig. 6, a–c). Importantly, all groups had equivalent neutrophil numbers in the spleen (Fig. 6 d), confirming that

GM-CSF signaling in the BM compartment is essential for infiltration into the heart but does not regulate neutrophils systemically. This finding demonstrates that GM-CSF does not signal directly on the parenchyma (which would include the endothelium) but, rather, acts on the BM compartment to drive cardiac inflammation. In keeping with an earlier study (Molawi et al., 2014), we confirmed that cardiac macrophages are replaced in BM chimeras (i.e., of donor origin; Fig. 6 e), suggesting the target of GM-CSF may be circulating granulocytes or cardiac macrophages. We therefore sought to determine whether GM-CSF signals directly on neutrophils
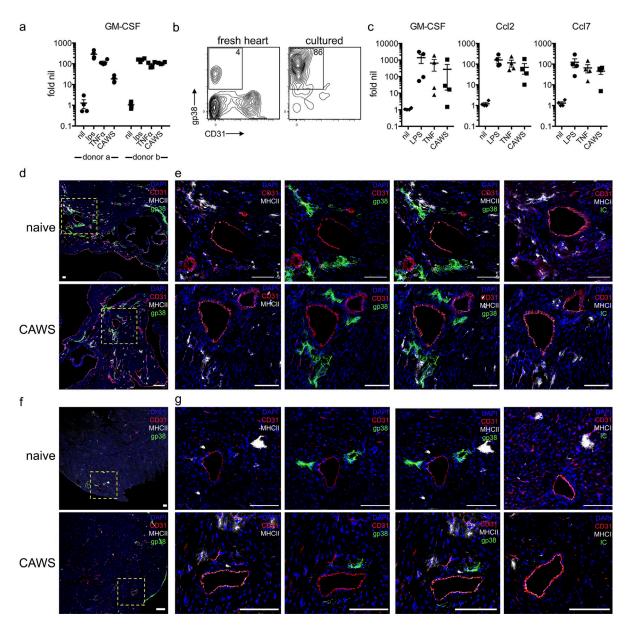
Figure 5. **Identifying activating stimuli and location of CFs.** (a) Primary human CFs were stimulated with LPS, TNF, or CAWS, and 4 h later, *GM-CSF* expression was measured by qPCR. Results show fold-induction relative to nil stimulation from two donors conducted over four experiments. (b) FACS analysis of B6 mouse hearts before and after in vitro culture. A representative contour plot of gp38 and CD31 expression is shown (inset value shows the mean from three individual CF lines). (c) Primary mouse CFs were stimulated with LPS, TNFα, or CAWS for 4 h, and *GM-CSF*, *Ccl2*, and *Ccl7* expression were measured by qPCR (values show gene expression relative to nil stimulation). The four data points represent individual experiments with different CF lines. (d–g) Hearts from naive and CAWS-injected (~20 h after challenge) RAG-1$^{-/-}$ mice were divided into upper (d and e) and lower (f and g) halves, stained for gp-38 (green), CD31 (red), and MHC-II (gray), and analyzed by confocal microscopy (isotype control [IC; green] of gp-38 antibody is shown). Yellow, dashed-lined boxes show image insets. Representative images of five to six mice from three experiments are shown. Bars, 100 µm.

and/or monocytes to regulate the intrinsic ability of these cells to migrate into the heart (i.e., by controlling homing receptor expression) or acted in a cell-extrinsic manner (i.e., by regulating the expression of neutrophil/monocyte-recruiting factors by cardiac macrophages). To distinguish between these two possibilities, we generated 50:50 mixed βc$^{-/-}$/WT BM chimeras (reconstituting B6.Ly5.1 hosts) to directly compare

the migration of WT (CD45.1$^+$) and βc$^{-/-}$ (CD45.2$^+$) cells in the same host during disease (Fig. 6 f). Here, we found that the ratio of WT to βc$^{-/-}$ neutrophils and monocytes was largely equivalent (Fig. 6 g) or somewhat skewed toward the βc$^{-/-}$ cells in the BM, demonstrating that neutrophil and monocyte development occurs independently of GM-CSF signaling. Second, the WT/βc$^{-/-}$ ratio for both neutrophils and mono-
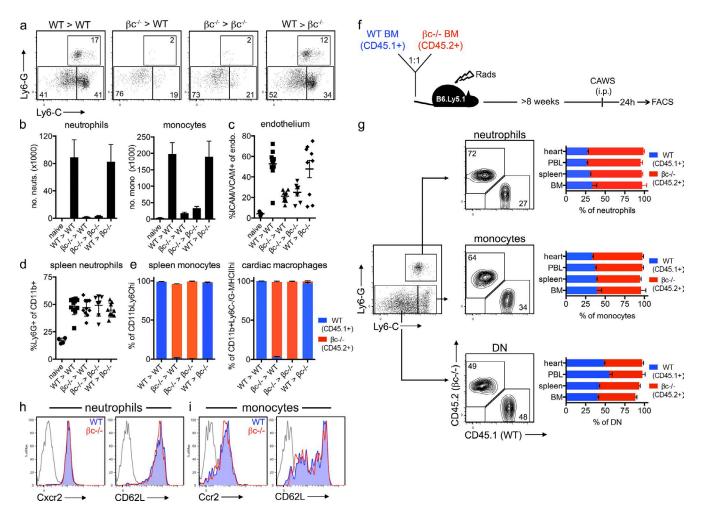
Figure 6. GM–CSF signaling on the hematopoietic compartment drives cardiac inflammation. (a–e) Reciprocal BM chimeras were generated with WT (B6.Ly5.1; CD45.1$^+$) and βc$^{-/-}$ (CD45.2$^+$) mice. BM chimeras were challenged with CAWS and 1 d later analyzed for the development of cardiac vasculitis. (a) Dot plots are gated on heart-resident (in vivo Gr-1$^-$) myeloid cells (CD11b$^+$). (b–e) Graphs depict the mean ± SEM number of neutrophils (neuts.) and monocytes (mono.) in the heart (b), ICAM/VCAM expression of cardiac endothelium (endo.; c), the frequency of neutrophils in the spleen (d), and the level of chimerism for splenic monocytes (CD11b$^+$Ly6G$^-$Ly6C^{hi}) and cardiac macrophages (CD11b$^+$Ly6C$^-$Ly6G$^-$MHCII^{hi}; e). Values are pooled from three to nine mice pooled from four experiments. (f and g) 50:50 mixed B6.Ly5.1 (CD45.1$^+$) + βc$^{-/-}$ (CD45.2$^+$) BM chimeras were challenged with CAWS, and 1 d later, WT and βc$^{-/-}$ neutrophils, monocytes, and double-negative (DN; Ly6C$^-$/G$^-$) macrophages were enumerated by flow cytometry. A representative dot plot of Ly6C and Ly6G expression is gated on resident (in vivo Gr-1$^-$) myeloid (CD11b$^+$) cells from the heart, with contour plots depicting the composition (B6.Ly5.1 vs. βc$^{-/-}$) of each population. Bar graphs show the frequency of each population across various organs (data represent the mean ± SEM of nine mice pooled from four experiments). (h and i) Homing receptor expression of WT (CD45.1$^+$) and βc$^{-/-}$ (CD45.2$^+$) neutrophils and monocytes isolated from the spleen of mixed B6.Ly5.1 + βc$^{-/-}$ BM chimeras 1 d after CAWS challenge. A representative histogram of six mice from two experiments is shown. WT, filled blue; βc$^{-/-}$, red line; and isotype control, gray line.

cytes was conserved across BM, spleen, PBL, and hearts in CAWS-challenged mice. This demonstrates that neutrophils and monocytes do not require GM-CSF signaling to egress from the BM to the circulation or from the circulation into the heart. Thus, GM-CSF functions independently of regulating neutrophil and monocyte development, BM egress, or the intrinsic ability to traffic into the heart. In keeping with equivalent tissue-entry capability, βc$^{-/-}$ and WT neutrophils and monocytes expressed similar levels of the chemokine receptors Cxcr2 and Ccr2, respectively, and the homing receptor CD62L (Fig. 6, h and i). Collectively, these data indicate

that GM-CSF acts on the BM compartment but does not signal directly on neutrophils and monocytes to regulate intrinsic homing capacity. Instead, we predict that GM-CSF acts in a cell-extrinsic manner, most likely via the activating cardiac macrophages to express factors that recruit neutrophils and monocytes into the heart.

GM-CSF drives cytokine and chemokine expression in cardiac macrophages

The findings shown in Fig. 6 suggest that GM-CSF activates cardiac inflammation by driving the expression of
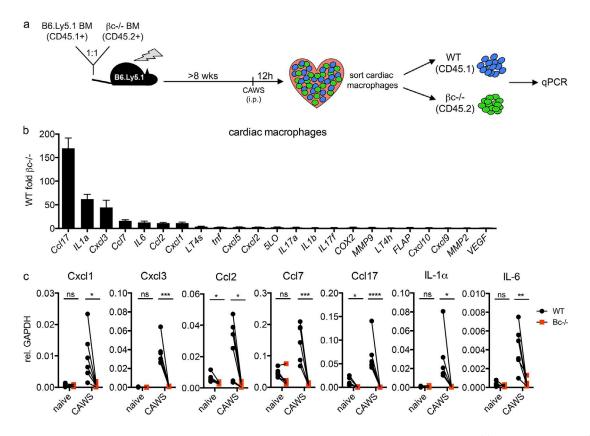
Figure 7.   **GM–CSF activates cardiac macrophages to express proinflammatory genes during cardiac vasculitis.** (a) 50:50 mixed B6.Ly5.1 (CD45.1$^+$) + βc$^{-/-}$ (CD45.2$^+$) BM chimeras were challenged with CAWS, and 12 h later, macrophages (CD11b$^+$Ly6G$^-$MHC II$^+$) were sorted from the heart into WT (CD45.1$^+$) and βc$^{-/-}$ (CD45.2$^+$) fractions and analyzed by qPCR. (b) The bar graph shows gene expression by WT relative to βc$^{-/-}$ macrophages (data represent mean ± SEM from five experiments). FLAP, 5-lipoxygenase activating protein; VEGF, vascular endothelial growth factor. (c) Graphs show the expression of target genes by WT and βc$^{-/-}$ cardiac macrophages sorted from naive or CAWS-challenged mixed B6.Ly5.1 (CD45.1$^+$) + βc$^{-/-}$ (CD45.2$^+$) BM chimeras (values indicate gene expression relative [rel.] to Gapdh and show paired samples pooled from five experiments). Statistical analysis was performed with unpaired, two-tailed Student's t tests. *, $P < 0.05$; **, $P < 0.01$; ***, $P < 0.001$; ****, $P < 0.0001$.

neutrophil and monocyte recruiting factors. We therefore identified which genes are directly regulated by GM-CSF in vivo during disease. Considering that GM-CSF signals on BM-derived cells (Fig. 6) yet lymphoid cells are dispensable for disease (Fig. 2), we reasoned that GM-CSF acted upon the myeloid compartment within the heart, with cardiac macrophages being the most likely candidates given their close proximity to CFs (Fig. 5). To enable the identification of GM-CSF target genes, we generated mixed βc$^{-/-}$/WT BM chimeras and performed a transcriptional comparison between WT (GM-CSF responsive) and βc$^{-/-}$ (GM-CSF nonresponsive) macrophages isolated from the same inflamed heart, reasoning that differentially expressed genes will be those that are directly regulated by GM-CSF. Chimeras were challenged with CAWs, and 12 h later, cardiac macrophages were sorted into WT and βc$^{-/-}$ fractions, and the expression of putative neutrophil and monocyte recruiting factors (chemokines, leukotriene-modifying enzymes, cytokines, and MMPs) were assessed by quantitative PCR (qPCR; Fig. 7 a). We identified several chemokines and cytokines that were overexpressed in WT compared

with βc$^{-/-}$ counterparts. Most notably, WT macrophages expressed significantly higher levels of the Ccr4 chemokine ligand *Ccl17* (∼150-fold), the Cxcr2 chemokine ligands *Cxcl1* (∼10-fold) and *Cxcl3* (∼45-fold), Ccr2 chemokine ligands *Ccl2* (∼10-fold) and *Ccl7* (∼20-fold), and cytokines *IL-1α* (∼60-fold) and *IL-6* (∼15-fold; Fig. 7 b). Critically, analysis of cardiac macrophages from naive mice showed those genes that were differentially expressed after CAWS challenge were expressed at low levels in the steady state and were not differentially expressed (with the exception of Ccl2 and Ccl17) between naive WT and βc$^{-/-}$ macrophages (Fig. 7 c). Thus, we have identified a panel of genes (*Cxcl1/3*, *Ccl2/7/17*, *IL-1α*, and *IL-6*) that are (a) expressed only during disease, and (b) only by cells that can respond to GM-CSF and, hence, can be considered directly regulated by GM-CSF in the heart during disease. These results elucidate the mechanism by which GM-CSF triggers cardiac inflammation, demonstrating that GM-CSF activates the local macrophage compartment to express proinflammatory cytokine and chemokines involved in immune cell recruitment to the heart and the elaboration of cardiac inflammation.
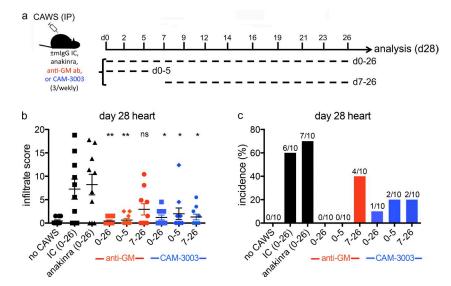
Figure 8. **Kinetic analysis of GM–CSF antagonism in CAWS–induced vasculitis.** (a) CAWS-challenged B6 mice received one of anakinra, anti–GM-CSF, anti–GM-CSF receptor (CAM-3003), or isotype control mAbs (mIgG IC; 0.25 mg, three time weekly) beginning at the time of challenge until day 26 (0–26), the time of challenge until day 5 (0–5), or starting at day 7 until day 26 (7–26). At day 28 after CAWS challenge, mice were sacrificed and assessed for cardiac inflammation by HE staining. (b and c) Bar graphs show cardiac disease severity (infiltrate score) and incidence. Data are pooled from two experiments with 10 mice per group. Statistical analysis was performed with unpaired, two-tailed Student's t tests. *, $P < 0.05$; **, $P < 0.01$.

Transient and therapeutic GM–CSF antagonism protects against secondary cardiac vasculitis in KD

Finally, we addressed the therapeutic potential of GM-CSF antagonism in KD. Here, we used two GM-CSF–blocking reagents: an anti–GM-CSF antibody or an anti–GM-CSF α receptor antibody (CAM-3003) that has previously been validated in an inflammatory arthritis model (Greven et al., 2015). For comparison, we also included anakinra, an IL-1 receptor antagonist. We challenged B6 mice with CAWS and analyzed cardiac inflammation at day 28, thereby evaluating the second wave of inflammatory disease that targets the coronary arteries and aortic root (Fig. 1). To compare the efficacy of therapeutic to prophylactic treatments, GM-CSF antagonists were administered throughout (day 0–26) or limited to the first week (day 0–5) or final 3 wk (day 7–26) after CAWS challenge (Fig. 8 a). As seen in Fig. 8, although anakinra did not protect against cardiac disease, both GM-CSF antagonists provided near complete protection when administered throughout (day 0–26). The anti–GM-CSF receptor antibody (CAM-3003) administered between days 0 and 5 or days 7 and 26 provided significant reduction in disease incidence and severity. In the case of the anti–GM-CSF antibody, administration between days 0 and 5 completely protected against the development of day 28 disease, whereas administration between days 7 and 26 provided some reduction in disease incidence and severity. Thus, despite minor differences between GM-CSF antagonists, these findings demonstrate that blocking GM-CSF either transiently during the initial stages alone (day 0–5) or over the final three weeks of disease (day 7–26) substantially reduces the development and severity of the second wave of cardiac disease. These findings demonstrate that the initial inflammatory myocarditis seen at day 1 is an essential priming event for the development of subsequent cardiac disease, providing an important insight into the progression of cardiac disease in KD. Our results also suggest that GM-CSF antagonism could represent a novel approach to the treatment of KD.

DISCUSSION

Neutrophils and monocytes are the major immune cell populations infiltrating the heart during KD (Takahashi et al., 2005; Harada et al., 2012) and are generally regarded as the cellular mediators of cardiac pathology (Suzuki et al., 2001; Takahashi et al., 2005). Consequently, understanding how the migration of these key cells is regulated during cardiac inflammation is of major relevance for improving therapy of KD and perhaps other types of vascular disease. We describe a novel role for GM-CSF as the primary initiator of these events. GM-CSF is rapidly and locally expressed within the heart during the initial stages of cardiac disease. GM-CSF functions to activate cardiac macrophages, which in turn promotes neutrophil and monocyte recruitment into the heart. Our findings identify GM-CSF as an essential inflammatory cytokine in the development of cardiac inflammation during KD.

We provide several lines of evidence that elucidate the mechanism by which GM-CSF drives cardiac inflammation. GM-CSF blockade at the time of CAWS challenge is sufficient to protect mice from developing cardiac inflammation, demonstrating that GM-CSF functions as an inflammatory cytokine in the context of this disease. In line with an inflammatory role, GM-CSF is rapidly and selectively expressed within the heart during the initial stages of disease, suggesting critical local activity. Indeed, we show that GM-CSF regulates cardiac but not systemic inflammation after CAWS challenge and specifically functions by stimulating the cardiac macrophage compartment to express a suite of proinflammatory genes. Notably, GM-CSF directly stimulates the expression of chemokines involved in immune cell migrations, including *Cxcl1/3* and *Ccl2/7*. These are ligands for Cxcr2 and Ccr2, respectively (Zlotnik and Yoshie, 2012), which are known to be expressed on neutrophils (Cxcr2) and monocytes (Ccr2) and, thus, are likely to be involved in controlling entry into the heart. Intriguingly, we also found that GM-CSF strongly regulated *Ccl17* expression. Although Ccl17 (a ligand for

Ccr4, a putative Th2 chemokine receptor) is not typically associated with neutrophil/monocyte migration, CCL17 expression and gene polymorphisms have been linked with KD susceptibility (Lee et al., 2013), indicating a potential role in KD. Collectively, our findings provide a detailed understanding into the mechanisms by which GM-CSF initiates cardiac disease, showing that GM-CSF is expressed and acts locally, switching on an inflammatory gene profile in resident macrophages of the heart.

GM-CSF has been widely reported to play a pathogenic role in several autoimmune diseases, including multiple sclerosis (MS) and rheumatoid arthritis (Cornish et al., 2009; Shiomi and Usui, 2015; Wicks and Roberts, 2016). Consequently, an important consideration is whether GM-CSF acts in a similar way in these diseases. In this regard, studies into the experimental autoimmune encephalomyelitis model of MS demonstrate that GM-CSF acts on monocytes to drive disease development (Ko et al., 2014; Croxford et al., 2015). These studies showed that Th17 cell–derived GM-CSF activates Ccr2$^+$ monocytes to express a proinflammatory gene signature (with targets including Ccl17 and Cxcl3) that exacerbates inflammation in the central nervous system (Croxford et al., 2015). We describe a similar mode of action for GM-CSF in the context of the heart in KD. In keeping with experimental autoimmune encephalomyelitis model, we show that GM-CSF does not signal directly to migratory inflammatory cells to regulate intrinsic homing capacity but instead functions within the tissue, activating inflammation by stimulating the expression of cytokines and chemokines by the local myeloid compartment. Thus, our findings provide some consensus as to the role of GM-CSF in tissue-specific autoimmune disease. Furthermore, several recent studies describe the dynamics and function of cardiac macrophages and highlight a central role for resident macrophages in regulating cardiac inflammation (Epelman et al., 2014a,b; Lavine et al., 2014; Molawi et al., 2014). Our data provide further support for such a role and demonstrate that GM-CSF is a major driver of this activity.

In contrast to diseases models of MS and inflammatory arthritis, where GM-CSF from autoreactive CD4$^+$ T cells is critical (Campbell et al., 2011; Codarri et al., 2011), we find that a population of CFs is the major source of GM-CSF production. Thus, whether GM-CSF is derived from tissue-infiltrating or resident sources appears context dependent. We show that CFs are rapidly activated upon CAWS challenge, as indicated by up-regulation of ICAM and VCAM, and respond via an initial cytokine (*GM-CSF/Ccl2/7*) burst. Importantly, the ability to produce GM-CSF is conserved in mouse and human CFs, arguing that CFs play a similar role in human cardiac physiology and disease. In this regard, it is important to note that our findings are in concert with observations that GM-CSF is essential for the development of T cell–mediated cardiomyopathy in a mouse model of myocarditis (Sonderegger et al., 2008). In that model, it was argued that GM-CSF acts via inducing IL-6 expression, a cytokine

that we show to be directly regulated by GM-CSF. Critically, CFs have recently been identified as the source of GM-CSF in this model of cardiomyopathy (Wu et al., 2014). Thus, our findings, together with these earlier studies, provide strong consensus that GM-CSF production by CFs is a central event in multiple inflammatory heart diseases.

One major question which arises from this work is how are CFs activated? In the study of T cell–mediated cardiomyopathy described in the previous paragraph (Wu et al., 2014), it was argued that IL-17 signaling activates CFs. However, we show that IL-17 is not essential for the development of cardiac disease in the CAWS model of KD. This is consistent with an earlier study demonstrating that IL-17α$^{-/-}$ mice develop typical cardiac disease in the *Lactobacillus casei* model of KD (Lee et al., 2012), arguing that IL-17 signaling does not play a major role in the activation of CFs in KD. In vitro, we show that human and mouse CFs produce GM-CSF in response to a range of stimuli, including LPS, TNF, and, to some degree, CAWS. Although these findings raise the possibility of CFs becoming activated by the direct recognition of the CAWS complex in vivo, further studies are required to determine whether this is the case or whether CFs respond to endogenous ligands such as cytokines or damage-associated molecular pattern molecules. A second key question is why CFs appear to be selectively activated in this model. Whether CFs are indeed unique in the capacity to respond to CAWS or respond in a unique fashion and whether it is these features that determine the cardiac tropism of the CAWs model of KD are the subjects of ongoing studies. Although heart-specific properties of CFs (compared with skin fibroblasts) have been identified (Furtado et al., 2014), whether these underpin their unique response to CAWS is unclear. However, an intriguing observation is the anatomical location of CFs. We show that CFs reside in close proximity to both blood vessels and macrophages within the heart. In this position, CFs would be ideally placed to both sense systemic alarms from the vasculature and activate proximal cardiac macrophages through GM-CSF production, thereby triggering local vasculitis. Thus, the ability of CFs to drive cardiac macrophage activation might, at least in part, be explained by their location within the heart.

Currently, KD is treated with high-dose, pooled human IgG, administered i.v. (IVIG). This is an important, albeit poorly understood, therapy that reduces the duration of fever and frequency of coronary artery abnormalities by ∼70–90% (Furusho et al., 1984; Newburger et al., 1986). However, fever persists in 10–15% of KD patients treated with IVIG, and 2–5% of KD patients still develop life-threatening coronary aneurysms (Newburger et al., 1986; Beiser et al., 1998; Burns et al., 1998; Sundel, 2015). As such, additional therapies to treat IVIG-resistant patients are required. In this regard, cytokine-targeting therapies are emerging as potential treatment options. We found that IL-1 antagonism had little effect, but blockade of GM-CSF signaling protected mice from the development of both initial and secondary phases of cardiac inflammation after CAWS, demonstrating the therapeutic potential for GM-CSF

antagonism in KD. These findings are particularly promising considering that several GM-CSF antagonists have now been developed and appear well tolerated and effective in clinical trials of rheumatoid arthritis (Shiomi and Usui, 2015; Wicks and Roberts, 2016). Therefore, targeting GM-CSF represents a clinically realistic treatment option for KD and, given the data we present, may be effective in limiting cardiac disease during KD.

Importantly, a kinetic analysis of GM-CSF antagonism revealed that both transient and therapeutic GM-CSF blockade impairs the development of the second wave of cardiac disease. These findings allow two important conclusions. First, blocking initial myocarditis prevents the development of subsequent cardiac disease that targets the aortic root and coronary arteries. Thus, the first wave of cardiac inflammation appears to be a priming event that triggers subsequent cardiac disease. Second, our finding that delayed GM-CSF antagonism, commencing 7 d after disease induction, was still effective in reducing secondary cardiac disease indicates that therapeutically targeting GM-CSF after the onset of KD may offer protection against disease progression. Thus, GM-CSF appears to be involved in both initial and subsequent waves of cardiac disease. However, given that CFs did not appear to be actively expressing GM-CSF at day 28 (i.e., the second wave of disease), whether GM-CSF acts similarly in the first and second wave of cardiac disease remains unclear. It is possible that GM-CSF is only transiently expressed during the activation phase of secondary disease (as is the case in the initial wave) and has already returned to basal levels by day 28 (by which time disease is established). Collectively, these findings provide mechanistic insight into cardiac disease in this experimental model of KD and support for the therapeutic potential of GM-CSF antagonism.

The prevailing view of KD etiology is that multiple viral, bacterial, or fungal (including *C. albicans*) pathogens trigger KD in genetically predisposed children. Hence, whether GM-CSF acts in a similar fashion when KD is triggered by alternate stimuli in humans is an important consideration. This is a potential limitation of our study, and ongoing research into the role of GM-CSF in alternate KD models and human disease will seek to address this issue. In summary, we have identified a novel role for GM-CSF in activating cardiac inflammation. In response to the inflammatory stimulus of CAWS, GM-CSF is selectively generated by a population of CFs and acts locally within the heart, driving local inflammatory gene expression by the cardiac macrophage compartment. The resulting cascade of chemokine production and adhesion molecule expression induces a distinctive pattern of cardiac inflammation. Our study provides significant new insights into how GM-CSF production results in organ-specific inflammation of the heart and implicates GM-CSF as a therapeutic target in the treatment of KD.

MATERIALS AND METHODS
Mice
C57BL/6 (B6), B6.SJL-PtprcaPep3b/BoyJ (B6.Ly5.1), IL-$1R^{-/-}$, IL-$6^{-/-}$, G-CSFR$^{-/-}$, GM-CSF$^{-/-}$, RAG-$1^{-/-}$, RAG2-common–γ-chain$^{-/-}$ (RAG-γC$^{-/-}$), and CSFRβ$^{-/-}$ (βc$^{-/-}$) mice were bred on a C57BL/6 background at the Walter and Eliza Hall Institute (WEHI). IL-17α$^{-/-}$ mice were provided by R. O'Donoghue (Latrobe University, Melbourne, Victoria, Australia). Mice were housed under specific pathogen-free conditions and used at 6–20 wk of age. For BM chimeras, recipient mice were irradiated (2 × 550 rads), injected i.v. with 5–10 × 10^6 donor BM cells, and allowed to reconstitute for at least 8 wk before use. All procedures in animal experiments were approved by the WEHI Animal Ethics Committee.

Induction of CAWS-induced KD
The CAWS complex was prepared based upon established methods (Nagi-Miura et al., 2006; Tada et al., 2008). In brief, *C. albicans* was grown in C-limiting media (pH 5.2 at 27°C) for 2 d. An equal volume of ethanol was added and allowed to stand overnight. The culture was centrifuged, and the pellet was dissolved in water. The complex was centrifuged, and the soluble fraction was mixed with an equal volume of ethanol and again allowed to stand overnight. The complex was centrifuged, and the pellet was dried in acetone. The resulting CAWS complex was dissolved in water and autoclaved before use. Mice were injected i.p. with 4 mg CAWS. Where indicated, mice received doses of 0.25 mg anti–GM-CSF mAb (22E9.11) or rat IgG2a isotype control antibody (WEHI antibody facility), anti–GM-CSF receptor α mAb (CAM-3003; Greven et al., 2015), mouse IgG isotype control (MedImmune), or Anakinra i.p. three times weekly after CAWS challenge.

Flow cytometry
For flow cytometric analysis, mice were injected i.v. with 2 µg anti–Gr-1 antibody (RB6-8C5; PE or APC-Cy7 conjugated) to label circulating granulocytes and sacrificed 10 min later. Mice were perfused, and organs were digested in 1 mg/ml type I collagenase (Worthington Biochemical Corporation) with 5 µg/ml DNase I (Sigma-Aldrich). Peritoneal samples were obtained by lavage and stained directly. Anti–mouse CD11b (M1/70), Gr-1 (RB6-8C5), Ly6C (AL-21), Ly6G (1A8), CD45.1 (A20), CD45.2 (104), CD64 (X54-5/71), MHC II (M5/114), CD31 (390), gp38 (eBio8.1.1), CD54/ICAM (YM/1.7.4), CD106/VCAM (4299), Cxcr2 (242216), Ccr2 (475301), and CD62L (MEL-14) directly conjugated mAbs (BD, eBioscience, or R&D Systems) were used for flow cytometry. Single-cell suspensions were washed and stained in PBS/2%FBS/2 mM EDTA. 100 ng/ml propidium iodide and 6–6.4 µm Sphero blank calibration beads (BD) were added immediately before analysis to stain dead cells and facilitate sample enumeration, respectively. Samples were acquired on a Fortessa flow cytometer (BD) and analyzed with FlowJo software (Tree Star).

Real-time qPCR
For quantitation of gene expression in tissues, hearts were harvested into RNAlater (Invitrogen), and tissue was homogenized on a Polytron homogenizer (Kinematica). RNA was

extracted using the RNeasy Micro kit (QIAGEN), and cDNA was synthesized with SuperScript III reverse transcriptase (Invitrogen) using oligo–deoxy thymidine primers (Promega). Real-time qPCR was performed with Fast Sybergren Master mix (Thermo Fisher Scientific) with the primers described in Table S1. For gene expression analysis of purified populations, cells were sorted on a FACSAria II flow cytometer (BD), and RNA and cDNA were prepared as above (Fig. 7) or with the Sybergreen Cells-to-Ct kit (Thermo Fisher Scientific; Fig. 4). qPCR was performed on a Viia7 PCR system (Thermo Fisher Scientific), gene expression was normalized to Gapdh (Δ cycle threshold [CT]), and values were shown either as target gene mRNA levels relative to Gapdh ($2^{-\Delta CT}$) or further calculated relative to a comparator ($2^{-\Delta\Delta CT}$).

Histology, IHC, and confocal microscopy
Hearts were dehydrated in 20% sucrose and frozen in optimal cutting temperature medium, and sections were fixed in acetone. For HE staining and IHC, 5-µM sections cut on coronal or transverse planes were stained with HE or biotinylated anti-Ly6G (clone 1A8), respectively. IHC was detected and developed with ABC reagent (Vector Laboratories) and DAB (Dako). For confocal microscopy, 12-µM sections were permeabilized with 0.1% Triton X-100 and blocked with 10% goat serum (Jackson ImmunoResearch Laboratories, Inc.), biotin/avidin, and Protein block (Dako). Sections were stained with anti-gp38 (eBio8.1.1; eBioscience), CD31 (MEC13.3; BD), and biotinylated anti–MHC II (M5/114; eBioscience) for detection with goat anti–hamster IgG AF488, goat anti–rat IgG AF594, and streptavidin 647, respectively (Thermo Fisher Scientific). Slides were counterstained with DAPI, and images were acquired on a confocal microscope (LSM-780; ZEISS) and analyzed with ImageJ software (National Institutes of Health). Inflammatory incidence and infiltrate score were assessed on 10 sequential transverse HE sections cut at 50-µM intervals descending through the aortic root. The calculated infiltrate score measured the depth and density of inflammatory cell infiltrate. Depth is the number of slides (out of 10) that had inflammatory cell infiltrate; density measures the mean area (mean %) of cardiac tissue with inflammatory cell infiltrate (mean % ÷ 10 = score out of 10). The two scores were combined to give a total out of 20. To evaluate disease incidence in some experiments, mice scoring three or more were deemed infiltrate positive. Sections were scored blinded to genotype and experimental group.

In vitro stimulation of CFs
Normal human ventricle CFs (Lonza) were grown in fibroblast basal medium supplemented with fibroblast growth factor B, insulin, gentamycin, and 10% fetal bovine serum. For mouse CFs, hearts were digested in collagenase I/DNase, plated into 6-well tissue culture plates, and grown in DMEM containing 20% fetal bovine serum, 50 U/ml penicillin, and 50 µg/ml streptomycin. CFs were used in experiments between two and five passages of generation. For assays, 10^4/well CFs were

plated into 96-well flat-bottom plates and rested overnight before stimulation with 50 ng/ml LPS (Sigma-Aldrich), 50 ng/ml TNF (PeproTech), or 1 mg/ml CAWS. After 4 h, RNA was extracted, and cDNA was synthesized with the Sybergreen Cells-to-Ct kit (Thermo Fisher Scientific) for qPCR.

Statistical analysis
Statistical analysis was performed with Prism 6.0 (GraphPad Software) using unpaired, two-tailed Student's t tests. *, $P < 0.05$; **, $P < 0.01$; ***, $P < 0.001$; ****, $P < 0.0001$.

Online supplemental material
Table S1 shows primer sequences used for real-time PCR. Online supplemental material is available at http://www.jem.org/cgi/content/full/jem.20151853/DC1.

REFERENCES
Beiser, A.S., M. Takahashi, A.L. Baker, R.P. Sundel, and J.W. Newburger. US Multicenter Kawasaki Disease Study Group. 1998. A predictive instrument for coronary artery aneurysms in Kawasaki disease. *Am. J. Cardiol.* 81:1116–1120. http://dx.doi.org/10.1016/S0002-9149(98)00116-7

Biezeveld, M.H., G. van Mierlo, R. Lutter, I.M. Kuipers, T. Dekker, C.E. Hack, J.W. Newburger, and T.W. Kuijpers. 2005. Sustained activation of neutrophils in the course of Kawasaki disease: an association with matrix metalloproteinases. *Clin. Exp. Immunol.* 141:183–188. http://dx.doi.org/10.1111/j.1365-2249.2005.02829.x

Brown, T.J., S.E. Crawford, M.L. Cornwall, F. Garcia, S.T. Shulman, and A.H. Rowley. 2001. CD8 T lymphocytes and macrophages infiltrate coronary artery aneurysms in acute Kawasaki disease. *J. Infect. Dis.* 184:940–943. http://dx.doi.org/10.1086/323155

Burns, J.C., E.V. Capparelli, J.A. Brown, J.W. Newburger, and M.P. Glode. US/Canadian Kawasaki Syndrome Study Group. 1998. Intravenous gamma-globulin treatment and retreatment in Kawasaki disease. *Pediatr. Infect. Dis. J.* 17:1144–1148. http://dx.doi.org/10.1097/00006454-199812000-00009

Campbell, I.K., A. van Nieuwenhuijze, E. Segura, K. O'Donnell, E. Coghill, M. Hommel, S. Gerondakis, J.A. Villadangos, and I.P. Wicks. 2011. Differentiation of inflammatory dendritic cells is mediated by NF-κB1–dependent GM-CSF production in CD4 T cells. *J. Immunol.* 186:5468–5477. http://dx.doi.org/10.4049/jimmunol.1002923

Codarri, L., G. Gyülvészi, V. Tosevski, L. Hesske, A. Fontana, L. Magnenat, T. Suter, and B. Becher. 2011. RORγt drives production of the cytokine GM-CSF in helper T cells, which is essential for the effector phase of

autoimmune neuroinflammation. *Nat. Immunol.* 12:560–567. http://dx .doi.org/10.1038/ni.2027

Cornish, A.L., I.K. Campbell, B.S. McKenzie, S. Chatfield, and I.P. Wicks. 2009. G-CSF and GM-CSF as therapeutic targets in rheumatoid arthritis. *Nat. Rev. Rheumatol.* 5:554–559. http://dx.doi.org/10.1038/ nrrheum.2009.178

Croxford, A.L., M. Lanzinger, F.J. Hartmann, B. Schreiner, F. Mair, P. Pelczar, B.E. Clausen, S. Jung, M. Greter, and B. Becher. 2015. The cytokine GM-CSF drives the inflammatory signature of CCR2$^+$ monocytes and licenses autoimmunity. *Immunity.* 43:502–514. http://dx.doi.org/10 .1016/j.immuni.2015.08.010

Dahdah, N. 2010. Not just coronary arteritis, Kawasaki disease is a myocarditis, too. *J. Am. Coll. Cardiol.* 55:1507. http://dx.doi.org/10.1016/j.jacc.2009 .11.067

Epelman, S., K.J. Lavine, A.E. Beaudin, D.K. Sojka, J.A. Carrero, B. Calderon, T. Brija, E.L. Gautier, S. Ivanov, A.T. Satpathy, et al. 2014a. Embryonic and adult-derived resident cardiac macrophages are maintained through distinct mechanisms at steady state and during inflammation. *Immunity.* 40:91–104. http://dx.doi.org/10.1016/j.immuni.2013.11.019

Epelman, S., K.J. Lavine, and G.J. Randolph. 2014b. Origin and functions of tissue macrophages. *Immunity.* 41:21–35. http://dx.doi.org/10.1016 /j.immuni.2014.06.013

Fujiwara, H., and Y. Hamashima. 1978. Pathology of the heart in Kawasaki disease. *Pediatrics.* 61:100–107.

Fujiwara, H., C. Kawai, and Y. Hamashima. 1978. Clinicopathologic study of the conduction systems in 10 patients with Kawasaki's disease (mucocutaneous lymph node syndrome). *Am. Heart J.* 96:744–750. http ://dx.doi.org/10.1016/0002-8703(78)90007-8

Furtado, M.B., M.W. Costa, E.A. Pranoto, E. Salimova, A.R. Pinto, N.T. Lam, A. Park, P. Snider, A. Chandran, R.P. Harvey, et al. 2014. Cardiogenic genes expressed in cardiac fibroblasts contribute to heart development and repair. *Circ. Res.* 114:1422–1434. http://dx.doi.org/10.1161/CIR CRESAHA.114.302530

Furusho, K., T. Kamiya, H. Nakano, N. Kiyosawa, K. Shinomiya, T. Hayashidera, T. Tamura, O. Hirose, Y. Manabe, T. Yokoyama, et al. 1984. High-dose intravenous gammaglobulin for Kawasaki disease. *Lancet.* 324:1055–1058. http://dx.doi.org/10.1016/S0140-6736(84)91504-6

Greven, D.E., E.S. Cohen, D.M. Gerlag, J. Campbell, J. Woods, N. Davis, A. van Nieuwenhuijze, A. Lewis, S. Heasmen, M. McCourt, et al. 2015. Preclinical characterisation of the GM-CSF receptor as a therapeutic target in rheumatoid arthritis. *Ann. Rheum. Dis.* 74:1924–1930. http:// dx.doi.org/10.1136/annrheumdis-2014-205234

Hamamichi, Y., F. Ichida, X. Yu, K.I. Hirono, K.I. Uese, I. Hashimoto, S. Tsubata, T. Yoshida, T. Futatani, H. Kanegane, and T. Miyawaki. 2001. Neutrophils and mononuclear cells express vascular endothelial growth factor in acute Kawasaki disease: its possible role in progression of coronary artery lesions. *Pediatr. Res.* 49:74–80. http://dx.doi.org/10 .1203/00006450-200101000-00017

Harada, M., Y. Yokouchi, T. Oharaseki, K. Matsui, H. Tobayama, N. Tanaka, K. Akimoto, K. Takahashi, M. Kishiro, T. Shimizu, and K. Takahashi. 2012. Histopathological characteristics of myocarditis in acute-phase Kawasaki disease. *Histopathology.* 61:1156–1167. http://dx.doi.org/10.1111/j.1365 -2559.2012.04332.x

Holman, R.C., E.D. Belay, K.Y. Christensen, A.M. Folkema, C.A. Steiner, and L.B. Schonberger. 2010. Hospitalizations for Kawasaki syndrome among children in the United States, 1997–2007. *Pediatr. Infect. Dis. J.* 29:483–488. http://dx.doi.org/10.1097/INF.0b013e3181cf8705

Kato, H., T. Sugimura, T. Akagi, N. Sato, K. Hashino, Y. Maeno, T. Kazue, G. Eto, and R. Yamakawa. 1996. Long-term consequences of Kawasaki disease. A 10- to 21-year follow-up study of 594 patients. *Circulation.* 94:1379–1385. http://dx.doi.org/10.1161/01.CIR.94.6.1379

Kawasaki, T. 1967. [Acute febrile mucocutaneous syndrome with lymphoid involvement with specific desquamation of the fingers and toes in children]. *Arerugi.* 16:178–222.

Kawasaki, T. 2006. Kawasaki disease. *Proc. Jpn. Acad., Ser. B, Phys. Biol. Sci.* 82:59–71. http://dx.doi.org/10.2183/pjab.82.59

Kerscher, B., J.A. Willment, and G.D. Brown. 2013. The Dectin-2 family of C-type lectin-like receptors: an update. *Int. Immunol.* 25:271–277. http ://dx.doi.org/10.1093/intimm/dxt006

Ko, H.J., J.L. Brady, V. Ryg-Cornejo, D.S. Hansen, D. Vremec, K. Shortman, Y. Zhan, and A.M. Lew. 2014. GM-CSF–responsive monocyte-derived dendritic cells are pivotal in Th17 pathogenesis. *J. Immunol.* 192:2202–2209. http://dx.doi.org/10.4049/jimmunol.1302040

Korematsu, S., Y. Ohta, N. Tamai, M. Takeguchi, C. Goto, H. Miyahara, T. Kawano, and T. Izumi. 2012. Cell distribution differences of matrix metalloproteinase-9 and tissue inhibitor of matrix metalloproteinase-1 in patients with Kawasaki disease. *Pediatr. Infect. Dis. J.* 31:973–974. http ://dx.doi.org/10.1097/INF.0b013e31825ba6b3

Lavine, K.J., S. Epelman, K. Uchida, K.J. Weber, C.G. Nichols, J.D. Schilling, D.M. Ornitz, G.J. Randolph, and D.L. Mann. 2014. Distinct macrophage lineages contribute to disparate patterns of cardiac recovery and remodeling in the neonatal and adult heart. *Proc. Natl. Acad. Sci. USA.* 111:16029–16034. http://dx.doi.org/10.1073/pnas.1406508111

Lee, C.P., Y.H. Huang, Y.W. Hsu, K.D. Yang, H.C. Chien, H.R. Yu, Y.L. Yang, C.L. Wang, W.C. Chang, and H.C. Kuo. 2013. TARC/CCL17 gene polymorphisms and expression associated with susceptibility and coronary artery aneurysm formation in Kawasaki disease. *Pediatr. Res.* 74:545–551. http://dx.doi.org/10.1038/pr.2013.134

Lee, Y., D.J. Schulte, K. Shimada, S. Chen, T.R. Crother, N. Chiba, M.C. Fishbein, T.J. Lehman, and M. Arditi. 2012. Interleukin-1β is crucial for the induction of coronary artery inflammation in a mouse model of Kawasaki disease. *Circulation.* 125:1542–1550. http://dx.doi.org/10 .1161/CIRCULATIONAHA.111.072769

Matsubara, T., S. Furukawa, and K. Yabuta. 1990. Serum levels of tumor necrosis factor, interleukin 2 receptor, and interferon-γ in Kawasaki disease involved coronary-artery lesions. *Clin. Immunol. Immunopathol.* 56:29–36. http://dx.doi.org/10.1016/0090-1229(90)90166-N

Molawi, K., Y. Wolf, P.K. Kandalla, J. Favret, N. Hagemeyer, K. Frenzel, A.R. Pinto, K. Klapproth, S. Henri, B. Malissen, et al. 2014. Progressive replacement of embryo-derived cardiac macrophages with age. *J. Exp. Med.* 211:2151–2158. http://dx.doi.org/10.1084/jem.20140639

Murata, H., and S. Naoe. 1987. Experimental *Candida*-induced arteritis in mice—relation to arteritis in Kawasaki disease. *Prog. Clin. Biol. Res.* 250:523.

Nagi-Miura, N., T. Harada, H. Shinohara, K. Kurihara, Y. Adachi, A. Ishida-Okawara, T. Oharaseki, K. Takahashi, S. Naoe, K. Suzuki, and N. Ohno. 2006. Lethal and severe coronary arteritis in DBA/2 mice induced by fungal pathogen, CAWS, *Candida albicans* water-soluble fraction. *Atherosclerosis.* 186:310–320. http://dx.doi.org/10.1016/j.atherosclerosis .2005.08.014

Naoe, S., K. Takahashi, H. Masuda, and N. Tanaka. 1991. Kawasaki disease. With particular emphasis on arterial lesions. *Acta Pathol. Jpn.* 41:785–797.

Newburger, J.W., M. Takahashi, J.C. Burns, A.S. Beiser, K.J. Chung, C.E. Duffy, M.P. Glode, W.H. Mason, V. Reddy, S.P. Sanders, et al. 1986. The treatment of Kawasaki syndrome with intravenous gamma globulin. *N. Engl. J. Med.* 315:341–347. http://dx.doi.org/10.1056/NEJM198608073150601

Ng, L.G., J.S. Qin, B. Roediger, Y. Wang, R. Jain, L.L. Cavanagh, A.L. Smith, C.A. Jones, M. de Veer, M.A. Grimbaldeston, et al. 2011. Visualizing the neutrophil response to sterile tissue injury in mouse dermis reveals a three-phase cascade of events. *J. Invest. Dermatol.* 131:2058–2068. http:// dx.doi.org/10.1038/jid.2011.179

Niwa, Y., and K. Sohmiya. 1984. Enhanced neutrophilic functions in mucocutaneous lymph node syndrome, with special reference to the possible role of increased oxygen intermediate generation in the

pathogenesis of coronary thromboarteritis. *J. Pediatr.* 104:56–60. http://dx.doi.org/10.1016/S0022-3476(84)80589-2

Onouchi, Y. 2012. Genetics of Kawasaki disease: What we know and don't know. *Circ. J.* 76:1581–1586. http://dx.doi.org/10.1253/circj.CJ-12-0568

Onouchi, Y., K. Ozaki, J.C. Burns, C. Shimizu, M. Terai, H. Hamada, T. Honda, H. Suzuki, T. Suenaga, T. Takeuchi, et al. US Kawasaki Disease Genetics Consortium. 2012. A genome-wide association study identifies three new risk loci for Kawasaki disease. *Nat. Genet.* 44:517–521. http://dx.doi.org/10.1038/ng.2220

Principi, N., D. Rigante, and S. Esposito. 2013. The role of infection in Kawasaki syndrome. *J. Infect.* 67:1–10. http://dx.doi.org/10.1016/j.jinf.2013.04.004

Saijo, S., S. Ikeda, K. Yamabe, S. Kakuta, H. Ishigame, A. Akitsu, N. Fujikado, T. Kusaka, S. Kubo, S.H. Chung, et al. 2010. Dectin-2 recognition of α-mannans and induction of Th17 cell differentiation is essential for host defense against *Candida albicans*. *Immunity.* 32:681–691. http://dx.doi.org/10.1016/j.immuni.2010.05.001

Senzaki, H. 2006. The pathophysiology of coronary artery aneurysms in Kawasaki disease: role of matrix metalloproteinases. *Arch. Dis. Child.* 91:847–851. http://dx.doi.org/10.1136/adc.2005.087437

Shiomi, A., and T. Usui. 2015. Pivotal roles of GM-CSF in autoimmunity and inflammation. *Mediators Inflamm.* 2015. http://dx.doi.org/10.1155/2015/568543

Sonderegger, I., G. Iezzi, R. Maier, N. Schmitz, M. Kurrer, and M. Kopf. 2008. GM-CSF mediates autoimmunity by enhancing IL-6–dependent Th17 cell development and survival. *J. Exp. Med.* 205:2281–2294. http://dx.doi.org/10.1084/jem.20071119

Stock, A.T., J.M. Smith, and F.R. Carbone. 2014. Type I IFN suppresses Cxcr2 driven neutrophil recruitment into the sensory ganglia during viral infection. *J. Exp. Med.* 211:751–759. http://dx.doi.org/10.1084/jem.20132183

Sundel, R.P. 2015. Kawasaki disease. *Rheum. Dis. Clin. North Am.* 41:63–73. http://dx.doi.org/10.1016/j.rdc.2014.09.010

Suzuki, H., E. Noda, M. Miyawaki, T. Takeuchi, S. Uemura, and M. Koike. 2001. Serum levels of neutrophil activation cytokines in Kawasaki disease. *Pediatr. Int.* 43:115–119. http://dx.doi.org/10.1046/j.1442-200x.2001.01362.x

Tada, R., N. Nagi-Miura, Y. Adachi, and N. Ohno. 2008. The influence of culture conditions on vasculitis and anaphylactoid shock induced by fungal pathogen *Candida albicans* cell wall extract in mice. *Microb. Pathog.* 44:379–388. http://dx.doi.org/10.1016/j.micpath.2007.10.013

Takahashi, K., T. Oharaseki, S. Naoe, M. Wakayama, and Y. Yokouchi. 2005. Neutrophilic involvement in the damage to coronary arteries in acute stage of Kawasaki disease. *Pediatr. Int.* 47:305–310. http://dx.doi.org/10.1111/j.1442-200x.2005.02049.x

Takahashi, K., T. Oharaseki, and Y. Yokouchi. 2011. Pathogenesis of Kawasaki disease. *Clin. Exp. Immunol.* 164:20–22. http://dx.doi.org/10.1111/j.1365-2249.2011.04361.x

Uehara, R., and E.D. Belay. 2012. Epidemiology of Kawasaki disease in Asia, Europe, and the United States. *J. Epidemiol.* 22:79–85. http://dx.doi.org/10.2188/jea.JE20110131

Wicks, I.P., and A.W. Roberts. 2016. Targeting GM-CSF in inflammatory diseases. *Nat. Rev. Rheumatol.* 12:37–48. http://dx.doi.org/10.1038/nrrheum.2015.161

Wu, L., S. Ong, M.V. Talor, J.G. Barin, G.C. Baldeviano, D.A. Kass, D. Bedja, H. Zhang, A. Sheikh, J.B. Margolick, et al. 2014. Cardiac fibroblasts mediate IL-17A–driven inflammatory dilated cardiomyopathy. *J. Exp. Med.* 211:1449–1464. http://dx.doi.org/10.1084/jem.20132126

Yoshimura, K., K. Tatsumi, A. Iharada, S. Tsuji, A. Tateiwa, M. Teraguchi, H. Ogino, and K. Kaneko. 2009. Increased nitric oxide production by neutrophils in early stage of Kawasaki disease. *Eur. J. Pediatr.* 168:1037–1041. http://dx.doi.org/10.1007/s00431-008-0872-1

Zlotnik, A., and O. Yoshie. 2012. The chemokine superfamily revisited. *Immunity.* 36:705–716. http://dx.doi.org/10.1016/j.immuni.2012.05.008